IEEE Access
Multidisciplinary | Rapid Review | Open Access Journal

Received April 28, 2022, accepted May 9, 2022, date of publication May 12, 2022, date of current version May 23, 2022.

Digital Object Identifier 10.1109/ACCESS.2022.3174572

Novel Graphene Allocating Carbon−Copper Ratio Method for the Rail Vehicle Propulsion System Ground Carbon Brush

LIANG-YIN HUANG[1], HWA-DONG LIU[2], SHIUE-DER LU[3], AND CHIH-MING HSU[1]

[1]Graduate Institute of Manufacturing Technology, National Taipei University of Technology, Taipei 106344, Taiwan
[2]Undergraduate Program of Vehicle and Energy Engineering, National Taiwan Normal University, Taipei 106209, Taiwan
[3]Department of Electrical Engineering, National Chin-Yi University of Technology, Taichung 411030, Taiwan

Corresponding author: Hwa-Dong Liu (hdliu@ntnu.edu.tw)

This work was supported in part by the National Taiwan Normal University (NTNU), Taiwan; and in part by the National Taiwan Normal University Subsidy Policy to Enhance Academic Research Projects.

ABSTRACT This study proposed graphene allocating carbon−copper ratio (GACCR) for the grounding carbon brush of rail vehicle propulsion systems. The proposed GACCR is the key component of grounding apparatuses, and the system effectiveness can be enhanced by increasing the electro−conductive efficiency of the grounding carbon brush. The proposed GACCR applies physical vapor deposition, which uses a sputtering system to control the vacuum and temperature, thereby adjusting the copper to carbon ratio, and fabricate optimized graphene. This study employed an energy dispersive spectrometer to observe the graphite flake corrugated stack architecture on the surface of grounding carbon brush, and analyze the composition. A four−point probe was used to measure the impedance characteristic. The characteristics of graphite film were detected using a Raman spectrometer. The G peak of 1580 cm^{-1} and the 2D peak at 2750 cm^{-1} formed the two−dimensional structure of graphite film. Finally, this study took the underground rail vehicle as an example. The grounding carbon brush with the proposed GACCR was compared with traditional graphite grounding carbon brush to assess the economic benefit of periodically changing the grounding carbon brush of rail vehicles every three years. The proposed GACCR can save 112000 USD (35% compared to the original replacement grounding carbon brush cost) for Taiwan Metro, proving its significant cost−benefit effect.

INDEX TERMS Graphene allocating carbon−copper ratio, grounding carbon brush, rail vehicle, two−dimensional structure, ramen spectroscopy.

I. INTRODUCTION

The technology and development of material industry have evolved from a rough structure, low efficiency, and large volume into a fine structure, high efficiency, and compactness. Although graphite material is extensively used in industries and people's life, its preparation process has safety risks, and faces problem of structural roughness. The application areas of graphene include electronic modules [1]–[3], artificial intelligence (AI) sensor modules [4], [5], medical detection components [6], [7], biomedical technology [8], communication devices [9]–[11], photovoltaic components [12], optical gas sensor modules [13], solar cells [14], ultrasonic technology [15], piezoelectric electrode technology [16], and metallic corrosion detection technique [17].

The existence of a two−dimensional carbon structure has been discussed in previous studies, which also suggested that the atomic disturbance in the thermodynamic theory induced the unstable existence of a two-dimensional structure. In 2004, Novoselov *et al.* [18] performed simple preparation at room temperature to prove the existence of two−dimensional carbon materials, called graphene. The Nobel Prize in Physics of 2010 was awarded for the foundation of graphene.

Graphene is a cellular lattice structure formed of bonded single−layer carbon atoms. Each carbon atom has three sp^2 hybrid orbitals. The adjacent carbon atom is σ bonded covalent bond, and the included angle between atoms is 120 °. Two

The associate editor coordinating the review of this manuscript and approving it for publication was Sudhakar Babu Thanikanti.

carbon atoms of the unit cell are the substrate; as the bond length between carbon atoms is 0.142 nm, the lattice constant is 0.246 nm according to the lattice vector. The hexagonal region enclosed by reciprocal lattice points is the first Brillouin zone of k space. The reciprocal lattice face of graphene can be calculated using Fast Fourier Transform (FFT) by tunneling current microscope or transmission microscope [19].

The tight−binding approximation model of the graphene. In the simulated electron energy band of single−layer graphene, there are two symmetrical energy bands on the k plane, meaning the π electronic orbital of a carbon atom and adjacent π electronic orbital are coupled to form π band. High energy is anti−bonding π band (π^* band), which is called conduction band; low energy is bonding π band (π band), which is called valance band. The valence and conduction band junction is Dirac point. The junction induces metallic and semiconductive semimetallic characteristics of graphene. This means that the energy band density of the Fermi level is zero. Therefore, graphene is also known as a zero−gap semiconductor [19].

There are multiple methods of producing graphene. Novoselov *et al.* [18] introduced mechanical exfoliation. The highly oriented pyrolytic graphite (HOPG) monocrystal material surface was affixed with scotch tape, and the HOPG affixed adhesive tape was folded and affixed. The graphene adsorbed on the 300 nm SiO_2 substrate due to Van der Waals force, and a stable two−dimensional carbon material could be found. This preparation method is easy, but it cannot prepare large−area graphene thin film. Only a few μm graphene thin films with a few layers can be fabricated. Later, Su *et al.* [20] introduced electrochemical exfoliation, in which high−quality graphene was exfoliated from graphite formation using an electrochemical method. This experiment used HOPG as the positive electrode and the carbon source to dissociate the graphene. It used platinum wire as the negative electrode and used a dilute sulfuric acid solution and potassium hydroxide solution as electrolytes. The defects in the graphene still exist as the induced oxidation reaction is ineffaceable, while drawing the sulfuric acid under the effect of anode potential. Tung *et al.* [21] introduced the oxidation−reduction method. The graphite flake oxide was put in the hydrazine (C_2H_4) solution, and the hydrazine solution concentration and composition were prepared to reduce the graphite flake oxide to flaky hydrazine−graphene suspended on the solution surface. Under the reduction reaction, the hydrazine−graphene could not completely disperse the graphite flake oxide. There was the bonding of NO_2 and N_2 on the edge of the dispersed flaky film due to reduction to reduce the ions adsorbed by hydrazine from graphite flake oxide. The preliminary problem of hydrazine−graphene was thus solved by ultrasonic oscillation, dilution, and centrifugal separation passivation. After coating hydrazine−graphene on SiO_2 substrate and the thermal annealing of hydrazine−graphene at 150 °C, the residual hydrazine was eliminated. The currently largest 20 μm × 40 μm single-layer graphene thin film was then formed. Hass *et al.* [22] studied SiC pyrolysis and used its substrate for pyrolysis. The graphite layer was formed on the surface of SiC in an ultrahigh vacuum environment at 1600 °C. The Si atom bond was broken and sublimed to depart from the surface. Graphite layers could only be formed from epitaxy through this graphitization [22]. Emtsev *et al.* [23] proposed an improved process method of pyrolyzing SiC in ultrahigh vacuum to form graphene film. The graphite film was formed by pyrolysis at high temperatures in the argon environment under 900 mbar. Their method could improve the surface smoothness of graphite film.

If the CVD preparation method for the graphene method uses rare metals such as Pt [24], Ru [25], and Ir [26] as catalysts and admits carbonaceous molecular gases like CH_4 and C_2H_2, the crystal face of metal could be catalyzed to grow the graphene film. However, the cost would be very high. Therefore, this study employed physical vapor deposition (PVD) to fabricate the graphene using Cu as a catalyst. The proposed method can grow graphene film with a large area. Under a vacuum, the surface morphology appears fine with fewer defects.

The remainder of this paper is organized as follows: Section II introduces the analysis and describes the graphene structure and material; Section III details the proposed graphene allocating carbon-copper ratio; Section IV presents the experimental results; Section V offers conclusions and suggests directions for future work.

II. ANALYSIS AND DESCRIPTION OF GRAPHENE STRUCTURE AND MATERIAL

Graphene is a hexagonal lattice arrangement of single−layer atoms, but thermodynamics influences the atom's disturbance which makes the surface fluctuate. Besides thermodynamic disturbance, different substrate and carbon atom bonding arrangements have different crystal orientations [27]. The two−layer graphene is formed by bonding single−layer atoms under Van der Waals force. The layers generate different stack modes under different interaction forces, among them are the atomic arrangement of AA−stacking; the atomic arrangement of AB−stacking; the stack mode of three−layer graphene with the atomic arrangement of ABC−stacking; the turbostratic stack mode and the spacing between layers is 0.34 nm [28].

Therefore, the graphene stack mode of single−layer atoms is affected by the atomic bonding of layers. The carbon atom arrangement of a triangular lattice is often observed in atomic lattice analysis.

This study took Taiwan's underground−rail−vehicle grounding carbon brush (GCB) as an example, and the traditional GCB material is graphite. The study changed the GCB material to graphene. Analysis and experimental validation were performed. The graphene is formed by carbon atom sp^2 bonding, and a hexagonal ring of a two−dimensional structure is formed. Carbon bonding is a steady covalent bonding. The physical and chemical properties are quite stable at ordinary temperatures; it is unlikely to generate lattice

defects making it a perfect carbon lattice structure. In terms of single−layer graphene, the electron transfer rate at ordinary temperature is more than 100 times that of Cu. The graphene is transparent, very thin, and has good electrical conductivity.

Graphene can have different structure types. The allotropes of carbon include zero−dimensional Buckyball, one−dimensional carbon nanotubes (CNTs), and two−dimensional graphite. These allotropes can be used in electronic modules [1], AI sensor modules [5], medical detection components [7], biomedical technology [8], communication devices [11], photovoltaic components [12], and solar cells [14].

To analyze the characteristics of the graphene, the band positions G−band and 2D−band of Raman spectrum are observed. The G−band peak of the graphene is at 1582 cm^{-1}, the 2D−band peak is at 2700 cm^{-1} (as shown in Figure 1). The distribution of peak position and strength varies with process conditions. The influential factors will be discussed according to the peak distribution of graphene. The G−band judges the performance of graphitization, and the 2D−band judges the number of layers of the graphene film. However, the ratio is the most direct way to judge single−layer graphene. The peak ratio of 2D−band to G−band below about 0.2 is the critical factor influencing the film−forming defect. The criteria for single−layer grapheme film are a peak ratio of the 2D−band to G−band about 1.5, and the 2D−band full width at half maximum (FWHM) smaller than 40 cm^{-1}. The 2D band distinguishes the number of graphene layers. The ratio of 2D−band to G−band decreases as the number of layers increases, and the bandwidth of FWHM increases with the number of layers [29].

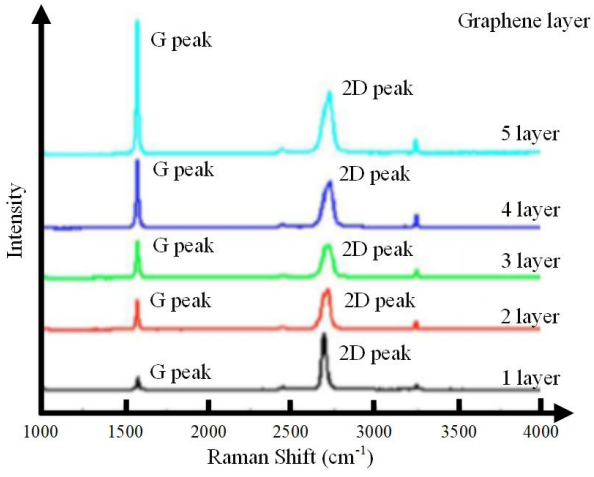

FIGURE 1. Curve diagram of Raman spectra of the graphene.

III. THE PROPOSED GRAPHENE ALLOCATING CARBON−COPPER RATIO

The graphene manufacturing method is physical vapor deposition (PVD), which uses the radio frequency sputter system, as shown in Figure 2. The Cu element in the graphene is in

FIGURE 2. The sputter system entity graph.

lattice mismatch with the carbon element. They are indissolvable in each other. The melting point of the Cu element is 1083 °C, and the melting point of the carbon element is 3827 °C, which influences the continuity of the graphite layer. The proposed graphene allocating carbon−copper ratio (GACCR) uses copper metal as a catalyst. The carbon atoms are diffused, separated out of copper metal, and rearranged to form hexagonal annular two−dimensional graphite. This is to obtain a large and smooth graphite layer. The addition of the Cu element contributes to the strength of graphite.

First, the radio frequency source (13.56 MHz) can negatively charge the insulator. The radio frequency can be added to both the front and back sides of the target by capacitance coupling. Second, the electrons are accelerated by high−frequency electric field variation, which affects the gas molecules to induce dissociation, generate glow discharge, and the plasma−excited atoms are generated. At this time, the ions in the plasma are attracted, and the ions of plasma dissociate and ionize the target electrode by ion bombardment due to reattraction. The reaction is excited to perform momentum transfer, thereby affecting the generation of ions, atoms, and more electrons by the target. Finally, when the ions and atoms in the plasma become stable, the gas flow makes the ions react with atoms to form atomic groups, and the atomic groups react with ions to form particles. The particles are nucleated and deposited to form a film.

Figure 2 displays the sputter system. The sputtering method is as folllows: the vacuum degree 7×10^{-3} torr is achieved by mechanic pump, and then the vacuum degree 3×10^{-6} torr is achieved by diffusion pump. The uniform and pure thin film is deposited in a high vacuum. The power is regulated by load voltage to change the particle deposition density to achieve thin film density.

The target material is copper metal in this study. The argon gas is not decomposed and impacted. A thin film is deposited

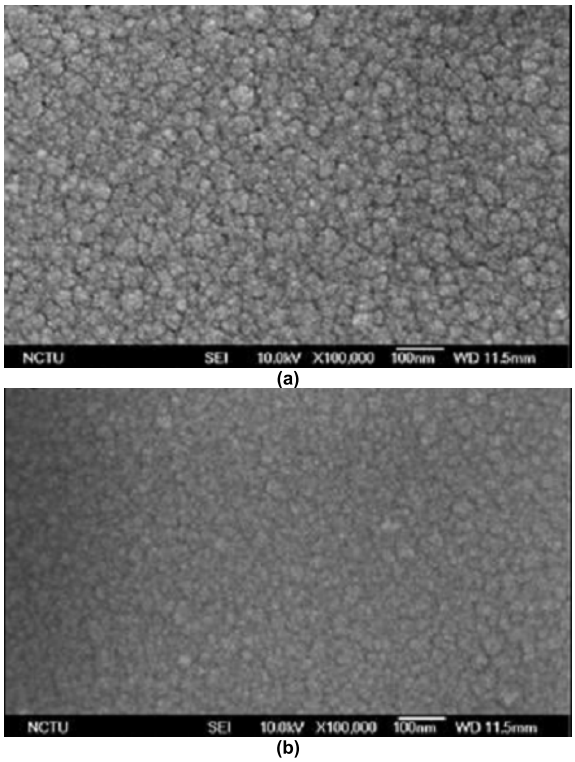

FIGURE 3. Deposited copper metal observed through thermal ionization scanning EDS: (a) 40W (b) 20W.

on SiO_2 substrate, and the deposition densities of different powers can be observed through the thermal ionization scanning energy dispersive spectrometer (EDS) (as shown in Figure 3). Figure 3 (a) shows the copper metal deposited under 40W. Figure 3 (b) shows the copper metal deposited under 20W.

In addition, the sputter system can perform a high−temperature thermal annealing process in a high vacuum (3×10^{-6}torr). The graphene sample has more defects as the thermal annealing process is performed under normal pressure in this experiment. This proves a steady growth of the proposed GACCR. The heater in the sputter system supports the bottom of the graphene sample. A current controller controls the temperature rise of a heater with a maximum temperature of 1200 °C. The actual heating temperature is accurately measured by a thermal couple device.

The steps of depositing copper atoms on the proposed GACCR substrate surface are described below. First, the oxide on the copper film surface is removed to form a structure of polycrystalline copper. Second, the methane or carbureted hydrogen gas is admitted. The copper film surface adsorbs carbon atoms. The copper film is a face−centered cubic (FCC) structure, but the copper and graphite have a good lattice match. A graphitized structure is formed on the copper surface, and amorphous carbon is formed on the other copper lattice faces. Over time, the amorphous carbon atoms and nearby graphite grow along with the copper film, generating a large graphite film. Third, copper and graphite have different thermal expansion coefficients in the cooling process, and they generate thermal stress. The graphite on the copper film surface grows wrinkles on the graphene layer to release the thermal stress. At last, it is observed through the EDS ionization scanning that the carbon atoms adhere to the transition metal surface on the proposed GACCR surface. Then the carbon atoms are diffused and separated out of the transition metal film surface. As transition metal catalysis at high temperatures aggregates graphite flakes, a smooth graphite film is formed.

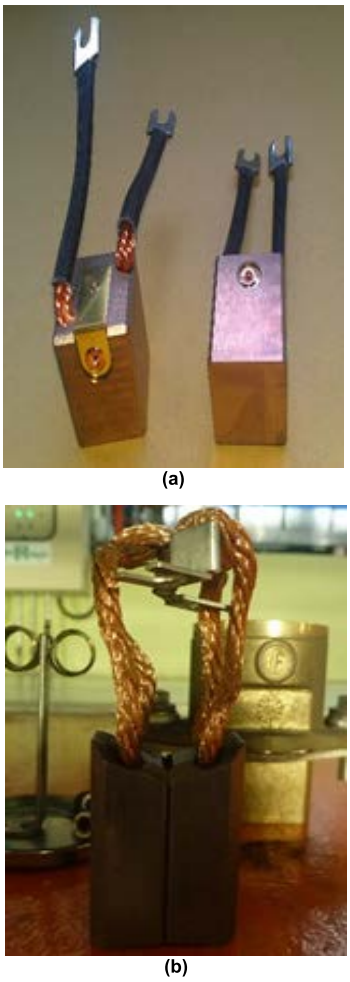

FIGURE 4. Stereogram of the proposed GACCR GCB for the rail vehicle propulsion system: (a) power car GCB (b) non−power car GCB.

IV. EXPERIMENTAL RESULTS

This study used transition metal to form catalysis at high temperatures. The carbon atoms passed through the copper transition metal, diffused, separated, and rearranged to form graphite to synthesize a large graphene layer to make the proposed GACCR. The proposed GACCR GCB was used in Taiwan's underground rail vehicles. Figure 4 shows the stereogram of the proposed GACCR GCB for the rail vehicle propulsion system. Figure 4 (a) is the stereogram of power car GCB. Figure 4 (b) is the stereogram of non−power car GCB. The testing instruments used in this study included thermal ionization scanning EDS (brand:

FIGURE 5. Thermal ionization scanning EDS.

FIGURE 6. Raman spectrometer.

FIGURE 7. Four-point probe instrument.

JEOL, model: JSM−6510LV), Raman spectrometer (brand: Donwo, specifications: laser source He−Cd, wavelength 532 nm), four−point probe (brand: KEITHLEY, model: 2400) for actual measurement and analysis, as shown in Figures 5 to 7.

Figure 8 shows the proposed GACCR power car GCB (as shown in Figure 4 (a)) morphology observed through ionization scanning EDS. Figure 8 (a) 100x morphology. Figure 8 (b) 2000x morphology.

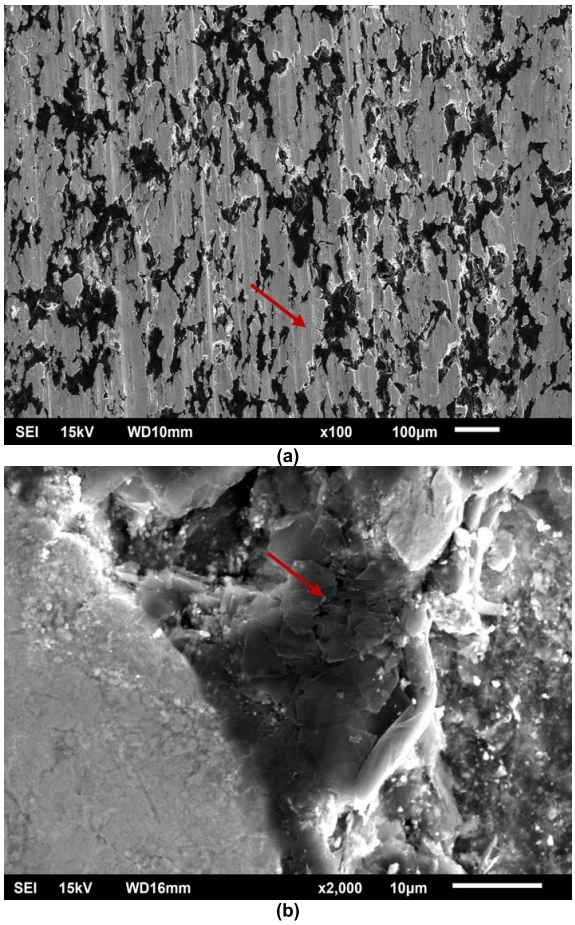

FIGURE 8. The proposed GACCR non-power car GCB morphology observed through ionization scanning EDS: (a) 100× morphology (b) 2000× morphology.

Figure 9 shows the proposed GACCR non−power car GCB (as shown in Figure 4 (b)) morphology observed through ionization scanning EDS. Figure 9 (a) shows 100x morphology, Figure 9 (b) shows 2000x morphology. Figures 8 and 9 show that the graphite in different directions is stacked together, describing the wrinkle stack architecture. The thermal stress released in the cooling process results in wrinkles, and the metal and graphite have different thermal expansion coefficients. Secondly, the wrinkle is formed due to different growth rates and temperature convection effects in different regions of the graphite layer. In addition, the number of graphite layers can be validated by Raman spectra.

Figure 10 shows the elements in the proposed GACCR power car GCB (as shown in Figure 4 (a)) region (Spectrum 26) selected by ionization scanning EDS. Figure 11 shows the spectral analysis of the elemental composition of the proposed GACCR power car GCB region (Spectrum 26). The elements include Cu, C, Pb, O, and Sn.

TABLE 1 displays the elemental composition analysis sheet of the proposed GACCR power car GCB. Cu Weight is 68.48 % and Atomic is 39.86 %; C Weight is 14.08 % and Atomic is 43.35 %; Pb Weight is 7.38 % and Atomic

TABLE 1. Elemental composition analysis sheet Of the proposed GACCR power car GCB.

Element	Weight %	Atomic %
Cu	68.48	39.86
C	14.08	43.35
Pb	7.38	1.32
O	6.17	14.26
Sn	3.89	1.21

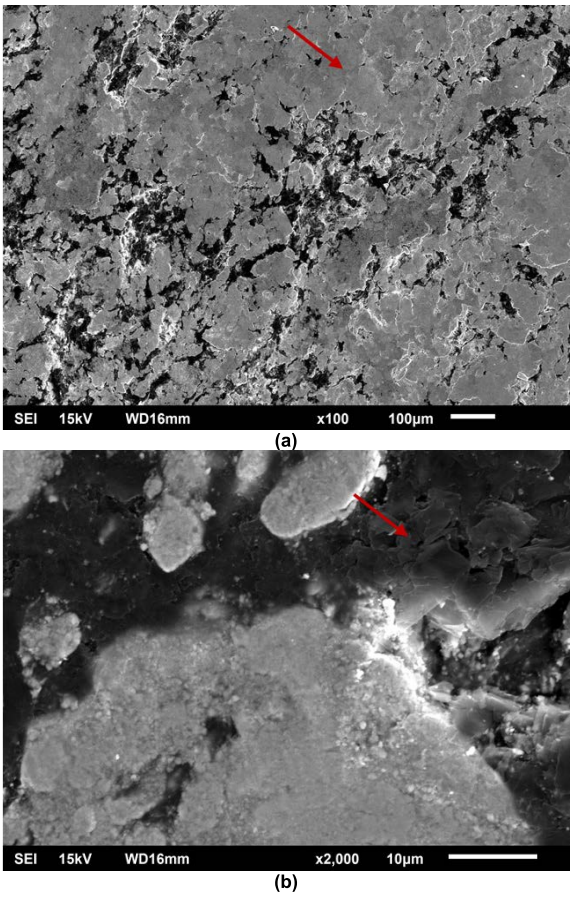

FIGURE 9. The proposed GACCR non− power car GCB morphology observed through ionization scanning EDS: (a) 100× morphology (b) 2000× morphology.

is 1.32 %; O Weight is 6.17 % and Atomic is 14.26 %; Sn Weight is 3.89 % and Atomic is 1.21 %.

Figure 12 shows the elements in the proposed GACCR non−power car GCB (as shown in Figure 4 (b)) region (Spectrum 23) selected by ionization scanning EDS. Figure 13 shows the spectral analysis of the elemental composition of the proposed GACCR non−power car GCB region (Spectrum 23). The elements include Cu, C, and O.

TABLE 2 shows the elemental composition analysis sheet of the proposed GACCR non−power car GCB. Cu Weight is 90.09 % and Atomic is 65.43 %; C Weight is 6.26 % and Atomic is 24.04 %; O Weight is 3.65 % and Atomic is 10.53 %.

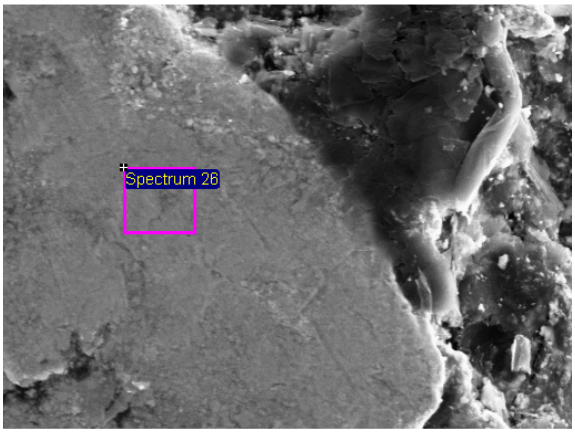

FIGURE 10. Elements in the proposed GACCR power car GCB region (Spectrum 26) selected by ionization scanning EDS.

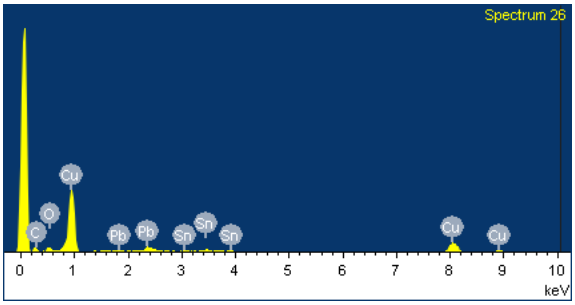

FIGURE 11. Spectral analysis of the elemental composition of the proposed GACCR power car GCB region (Spectrum 26).

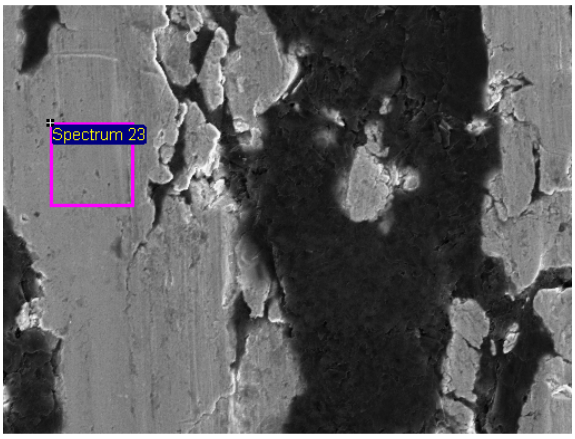

FIGURE 12. Elements in the proposed GACCR non−power car GCB region (Spectrum 23) selected by ionization scanning EDS.

TABLE 2. Elemental composition analysis sheet Of the proposed GACCR non−power car GCB.

Element	Weight %	Atomic %
Cu	90.09	65.43
C	6.26	24.04
O	3.65	10.53

The proposed GACCR was used for the rail vehicle propulsion system GCB. As the power car requires better electrical conductivity, the Cu weight of power car GCB is different from that of non−power car GCB. The power car's GCB Cu

TABLE 3. A four−point probe measured the proposed GACCR power car and non−power Car GCB impedance values.

Grounding carbon brush	1st test	2nd test	3rd test	4th test	5th test
Power car GCB impedance value	2.29510e-3 Ω	2.32185e-3 Ω	2.19063e-3 Ω	2.20449e-3 Ω	2.17068e-3 Ω
Non−power car GCB impedance value	2.10525e-3 Ω	2.05863e-3 Ω	2.14364e-3 Ω	2.25798e-3 Ω	2.28012e-3 Ω

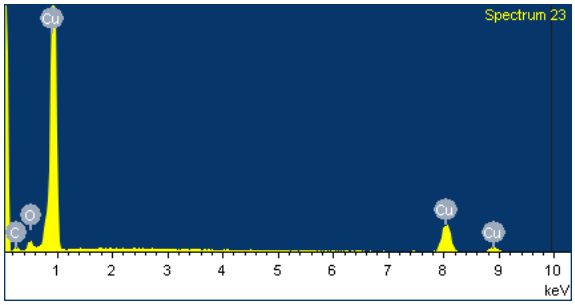

FIGURE 13. Spectral analysis of the elemental composition of the proposed GACCR non−power car GCB region (Spectrum 23).

weight is 68.48 % (as shown in TABLE 1), the non−power car's GCB Cu weight is 90.09 % (as shown in TABLE 2). The power car GCB Cu weight is lower than non−power car GCB therefore, the electrical conductivity is better.

TABLE 3 displays the proposed GACCR power car and non−power car GCB impedance values measured by a four−point probe. The power car GCB impedance value is measured five times, which is $2.29510e^{-3}\Omega$ at the first time, $2.32185e^{-3}\Omega$ at the second time, $2.19063e^{-3}\Omega$ at the third time, $2.20449e^{-3}\Omega$ at the fourth time, and $2.17068e^{-3}\Omega$ at the fifth time. The average value is $2.23655e^{-3}\Omega$. The non-power car GCB impedance value is measured five times, which is $2.10525e^{-3}\Omega$ at the first time, $2.05863e^{-3}\Omega$ at the second time, $2.14364e^{-3}\Omega$ at the third time, $2.25798e^{-3}\Omega$ at the fourth time, and $2.28012e^{-3}\Omega$ at the fifth time. The average value is $2.169124e^{-3}\Omega$. The proposed GACCR power car and non−power car GCB impedance values measured by the four−point probe are low, and the difference is minimal.

Figure 14 shows the Raman spectrogram of the proposed GACCR GCB. Figure 14 (a) shows the Raman spectrogram of power car GCB. Figure 14 (b) is the Raman spectrogram of non−power car GCB. In the actual measurement, the G peak of Figures 14 (a) and (b) is at 1580 cm^{-1}, and the 2D peak is at 2750 cm^{-1}. This proves that the proposed GACCR GCB is composed of a two−dimensional structure of graphite film. There is a good degree of graphitization and good lubricating effect, and the produced graphene is of high quality.

TABLE 4 demonstrates the costs of two GCBs. This study took Taiwan's underground rail vehicles as examples. Each

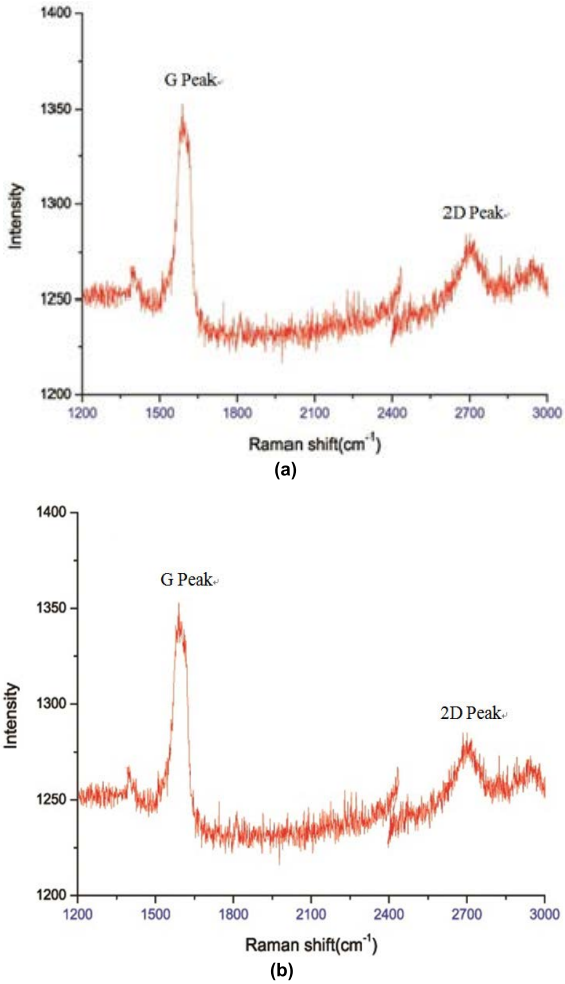

FIGURE 14. Raman spectrogram of the proposed GACCR GCB: (a) power car GCB (b) non−power car GCB.

TABLE 4. Cost comparison between two GCBs.

Material	Cost per GCB	GCB material cost per train	Fifty trains GCB material cost
Proposed GACCR	130 USD	4160 USD	208000 USD
Graphite	200 USD	6400 USD	320000 USD

train travels 121,000 km annually, and the annual wear of GCB is 0.6mm. The road life of each GCB is 390,000 km with an estimated lifetime of three years. Each GACCR GCB costs 130 USD, and each train has 32 GCBs which makes the total cost of 4160 USD. Each graphite GCB is 200 USD, totaling 6400 USD per train. The proposed GACCR GCB can save 2240 USD for each train. Fifty trains of the GCB underground−rail−vehicle were considered for this study. The total reduction in cost is 112000 USD. In other words, save 35% compared to the original replacement GCB cost which proves a significant cost-benefit.

V. CONCLUSION

The proposed GACCR used PVD and Cu as a catalyst. The PVD uses a sputtering system to control the vacuum and temperature, and adjust the copper to carbon ratio to fabricate optimized graphene. A large-area graphene film can be grown, which is fabricated in a vacuum. The surface morphology is relatively fine. The carbon and Cu element ratios of the proposed GACCR GCB were analyzed by ionization scanning EDS. A four-point probe measured the impedance values of graphene, and found that the graphene has low impedance. Finally, the G peak at 1580 cm^{-1} and the 2D peak at 2750 cm^{-1} were verified by Raman spectrum analysis, which were composed of the two-dimensional structure of graphite film. There is a good degree of graphitization and a good lubricating effect, which proves that the produced graphene has high quality.

The proposed GACCR GCB was used in Taiwan Metro's rail vehicle propulsion system, and its feasibility was verified. It was also compared with traditional graphite GCB, and the proposed GACCR could save 112000 USD for Metro Corp. every three years. In other words, save 35% compared to the original replacement GCB cost. Therefore, the proposed GACCR has feasibility and significant cost-benefit.

The future work will establish the optimum mixing ratio of copper and carbon in graphene, as well as related data and specifications to further reduce the GCB procurement cost. In addition, graphene material can be applied to other components of rail vehicles. This study contributes to enhancing the material effectiveness and reduces the maintenance cost of rail vehicles.

REFERENCES

[1] M. R. R. Abdul-Aziz, A. Hassan, A. A. R. Abdel-Aty, M. R. Saber, R. Ghannam, B. Anis, H. Heidari, and A. S. G. Khalil, "High performance supercapacitor based on laser induced graphene for wearable devices," *IEEE Access*, vol. 8, pp. 200573–200580, 2020, doi: 10.1109/ACCESS.2020.3035828.

[2] V. Vandeginste, "A review of fabrication technologies for carbon electrode-based micro-supercapacitors," *Appl. Sci.*, vol. 12, pp. 862–889, Jan. 2022, doi: 10.3390/app12020862.

[3] C. K. Hayashi, D. G. Garmire, T. J. Yamauchi, C. M. Torres, and R. C. Ordonez, "High on-off ratio graphene switch via electrical double layer gating," *IEEE Access*, vol. 8, pp. 92314–92321, 2020, doi: 10.1109/ACCESS.2020.2994611.

[4] M. Kachniarz, O. Petruk, W. Strupiński, T. Ciuk, A. Bieńkowski, R. Szewczyk, and J. Salach, "Quasi-free-standing bilayer graphene Hall-effect sensor," *IEEE Trans. Magn.*, vol. 55, no. 1, pp. 4000204–4000207, Jan. 2019, doi: 10.1109/TMAG.2018.2874070.

[5] D. Izci, C. Dale, N. Keegan, and J. Hedley, "The construction of a graphene Hall effect magnetometer," *IEEE Sensors J.*, vol. 18, no. 23, pp. 9534–9541, Dec. 2018, doi: 10.1109/JSEN.2018.2872604.

[6] S. Damiati, S. Søpstad, M. Peacock, A. S. Akhtar, I. Pinto, R. R. G. Soares, and A. Russom, "Flex printed circuit board implemented graphene-based DNA sensor for detection of SARS-CoV-2," *IEEE Sensors J.*, vol. 21, no. 12, pp. 13060–13067, Jun. 2021, doi: 10.1109/JSEN.2021.3068922.

[7] R. Lu, M. R. Haider, S. Gardner, J. I. D. Alexander, and Y. Massoud, "A paper-based inkjet-printed graphene sensor for breathing-flow monitoring," *IEEE Sensors Lett.*, vol. 3, no. 2, Feb. 2019, Art. no. 6000104, doi: 10.1109/LSENS.2018.2885316.

[8] B. Salesa, A. T.-Molina., A. C.-Vicent., M. Assis, J. Andrés, and S.-Aroca, "Graphene nanoplatelets: *In vivo* and *in vitro* toxicity, cell proliferative activity, and cell gene expression," *Appl. Sci.*, vol. 12, pp. 720–732, Jan. 2022, doi: 10.3390/app12020720.

[9] L. P. Shi, Q. H. Zhang, S. H. Zhang, C. Yi, and G. X. Liu, "Efficient graphene reconfigurable reflectarray antenna electromagnetic response prediction using deep learning," *IEEE Access*, vol. 9, pp. 22671–22678, 2021, doi: 10.1109/ACCESS.2021.3054944.

[10] B. Zhang, J. M. Jornet, I. F. Akyildiz, and Z. P. Wu, "Mutual coupling reduction for ultra-dense multi-band plasmonic nano-antenna arrays using graphene-based frequency selective surface," *IEEE Access*, vol. 7, pp. 33214–33225, 2019, doi: 10.1109/ACCESS.2019.2903493.

[11] S. Yan, J. Adcock, and Y. Ding, "Graphene on silicon photonics: Light modulation and detection for cutting-edge communication technologies," *Appl. Sci.*, vol. 12, pp. 313–324, Dec. 2021, doi: 10.3390/app12010313.

[12] Y. Wang, L. Lei, J. Zang, W. Dong, X. Zhang, and P. Xu, "High efficiency electro-optic modulation in a graphene silicon hybrid tapered microring resonator," *IEEE Access*, vol. 9, pp. 87869–87876, 2021, doi: 10.1109/ACCESS.2021.3089465.

[13] J. Wang, X. Zhang, Z. Wei, H. Qiu, Y. Chen, Y. Geng, Y. Du, Z. Cheng, and X. Li, "Design of a dual-mode graphene-on-microring resonator for optical gas sensing," *IEEE Access*, vol. 9, pp. 56479–56485, 2021, doi: 10.1109/ACCESS.2021.3072134.

[14] M. Kim, N. T. N. Truong, N. H. Lam, N. Le, A. M. Tamboli, M. S. Tamboli, T. N. L. Vu, and J. H. Jung, "Vacuum-free quantum dots planar hybrid solar cells: Improving charge transport using reduced graphene oxide and PEO as the buffer layer," *Appl. Sci.*, vol. 12, pp. 1185–1194, Jan. 2022, doi: 10.3390/app12031185.

[15] H. Mao, S. Lan, H. Mao, J. Ren, X. Yi, Z. Huang, and X. Li, "Experimental study on properties of ultrasonic coupling agent with graphene in NDT," *Appl. Sci.*, vol. 12, pp. 1236–1246, Jan. 2022, doi: 10.3390/app12031236.

[16] J. Chen, R. Han, D. Liu, and W. Zhang, "Active flutter suppression and aeroelastic response of functionally graded multilayer graphene nanoplatelet reinforced plates with piezoelectric patch," *Appl. Sci.*, vol. 12, pp. 1244–1261, Jan. 2022, doi: 10.3390/app12031244.

[17] M. Chakik, S. Bebe, and R. Prakash, "Hydrogenated graphene based organic thin film transistor sensor for detection of chloride ions as corrosion precursors," *Appl. Sci.*, vol. 12, pp. 863–874, Jan. 2022, doi: 10.3390/app12020863.

[18] K. S. Novoselov, A. K. Geim, S. V. Morozov, D. Jiang, Y. Zhang, S. V. Dubonos, I. V. Grigorieva, and A. A. Firsov, "Electric field effect in atomically thin carbon films," *Science*, vol. 306, no. 5696, pp. 666–669, Oct. 2004, doi: 10.1126/science.1102896.

[19] A. H. Castro Neto, F. Guinea, N. M. R. Peres, K. S. Novoselov, and A. K. Geim, "The electronic properties of graphene," *Rev. Modern Phys.*, vol. 81, no. 1, pp. 109–162, Feb. 2009.

[20] C.-Y. Su, A.-Y. Lu, Y. Xu, F.-R. Chen, N. A. Khlobystov, and L.-J. Li, "High-quality thin graphene films from fast electrochemical exfoliation," *ACS Nano*, vol. 5, no. 3, pp. 2332–2339, Feb. 2011, doi: 10.1021/nn200025p.

[21] V. C. Tung, M. J. Allen, Y. Yang, and R. B. Kaner, "High-throughput solution processing of large-scale graphene," *Nature Nanotechnol.*, vol. 4, no. 1, pp. 25–29, Nov. 2008.

[22] J. Hass, W. A. D. Heer, and E. H. Conrad, "The growth and morphology of epitaxial multilayer graphene," *J. Phys.*, vol. 20, no. 32, pp. 1–27, Jul. 2008, doi: 10.1088/0953-8984/20/32/323202.

[23] K. V. Emtsev, A. Bostwick, K. Horn, J. Jobst, G. L. Kellogg, L. Ley, J. L. McChesney, T. Ohta, S. A. Reshanov, J. Röhrl, E. Rotenberg, A. K. Schmid, D. Waldmann, H. B. Weber, and T. Seyller, "Towards wafer-size graphene layers by atmospheric pressure graphitization of silicon carbide," *Nature Mater.*, vol. 8, no. 3, pp. 203–207, Feb. 2009.

[24] P. Sutter, J. T. Sadowski, and E. Sutter, "Graphene on Pt(111): Growth and substrate interaction," *Phys. Rev. B, Condens. Matter*, vol. 80, no. 24, Dec. 2009, 245411, doi: 10.1103/PhysRevB.80.245411.

[25] S. Marchini, S. Günther, and J. Wintterlin, "Scanning tunneling microscopy of graphene on Ru(0001)," *Phys. Rev. B, Condens. Matter*, vol. 76, no. 7, Aug. 2007, Art. no. 075429, doi: 10.1103/PhysRevB.76.075429.

[26] J. Coraux, A. T. N'Diaye, C. Busse, and T. Michely, "Structural coherency of graphene on Ir(111)," *Nano Lett.*, vol. 8, no. 2, pp. 565–570, Jan. 2008, doi: 10.1021/nl0728874.

[27] J. C. Meyer, A. K. Geim, M. I. Katsnelson, K. S. Novoselov, T. J. Booth, and S. Roth, "The structure of suspended graphene sheets," *Nature*, vol. 446, pp. 60–63, Mar. 2007.

[28] A. N. Kolmogorov and V. H. Crespi, "Registry-dependent interlayer potential for graphitic systems," *Phys. Rev. B, Condens. Matter*, vol. 71, no. 23, Jun. 2005, Art. no. 235415, doi: 10.1103/PhysRevB.71.235415.

[29] I. Calizo, I. Bejenari, M. Rahman, G. Liu, and A. A. Balandin, "Ultraviolet Raman microscopy of single and multilayer graphene," *J. Appl. Phys.*, vol. 106, Aug. 2009, Art. no. 043509, doi: 10.1063/1.3197065.

LIANG-YIN HUANG received the M.S. degree from the National Taipei University of Technology, Taipei, Taiwan, in 2015, where he is currently pursuing the Ph.D. degree with the Graduate Institute of Manufacturing Technology. Since 1999, he has been a Group Chief at Metro Taipei. His primary research interests include materials engineering, rail vehicles, and solar energy engineering.

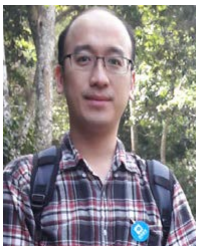

HWA-DONG LIU received the M.S. degree from Chung Yuan Christian University, Taoyuan, Taiwan, in 2006, and the Ph.D. degree from the National Taiwan University of Science and Technology, Taipei, Taiwan, in 2020. From April 2008 to July 2021, he was a Group Chief at Metro Taipei. Since August 2021, he has been with the Undergraduate Program of Vehicle and Energy Engineering, National Taiwan Normal University, Taipei, where he is currently an Assistant Professor. His primary research interests include power electronics for electric vehicle applications and solar energy.

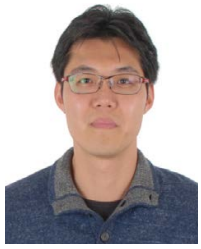

SHIUE-DER LU received the M.S. degree in electrical engineering from Chung Yuan Christian University (CYCU), in 2006, and the Ph.D. degree in electrical engineering from the National Taiwan University of Science and Technology (NTUST), in 2013. Since 2018, he has been with the Department of Electrical Engineering, National Chin-Yi University of Technology (NCUT), where he is currently an Associate Professor. His research interests include renewable energy, power systems, fault diagnosis, and optimization algorithm.

CHIH-MING HSU received the Ph.D. degree in electrical engineering from the National Taiwan University, Taipei, Taiwan, in 2013. He is currently an Associate Professor at the Department of Mechanical Engineering, National Taipei University of Technology, Taipei. His research interests include intelligent vehicles, intelligent transportation systems, and scene understanding for mobile robot. In 2011, he has received the Student Best Paper Award at IEEE International Conference on System Science and Engineering. In 2012, he has received the Best Paper Award at IEEE International Conference on System Science and Engineering. In 2013, he has received the Best Annual Paper Award sponsored by the Intelligent Transportation Society of Taiwan.